Nonlinear vibrational-state excitation and piezoelectric energy conversion in harmonically driven granular chains

C. Chong, E. Kim, E. G. Charalampidis, H. Kim, F. Li, P. G. Kevrekidis, J. Lydon, C. Daraio, and J. Yang

Nonlinear vibrational state excitation and piezoelectric energy conversion in harmonically driven granular chains

C. Chong*,[1,2] E. Kim,[3] E. G. Charalampidis,[4] H. Kim,[3]
F. Li,[3] P. G. Kevrekidis,[4] J. Lydon,[1] C. Daraio,[5] and J. Yang[3]

[1]*Department of Mechanical and Process Engineering (D-MAVT),*
Swiss Federal Institute of Technology (ETH), 8092 Zürich, Switzerland
[2]*Department of Mathematics, Bowdoin College, Brunswick, ME 04011, USA*
[3]*Aeronautics & Astronautics, University of Washington, Seattle, WA 98195-2400, USA*
[4]*Department of Mathematics and Statistics, University of Massachusetts, Amherst, MA 01003-4515, USA*
[5]*Department of Mechanical and Process Engineering (D-MAVT),*
Swiss Federal Institute of Technology (ETH), 8092 Zürich, Switzerland
Division of Engineering and Applied Science,
California Institute of Technology, Pasadena, CA, USA
(Dated: March 22, 2016)

This article explores the excitation of different vibrational states in a spatially extended dynamical system through theory and experiment. As a prototypical example, we consider a one-dimensional packing of spherical particles (a so-called granular chain) that is subject to harmonic boundary excitation. The combination of the multi-modal nature of the system and the strong coupling between the particles due to the nonlinear Hertzian contact force leads to broad regions in frequency where different vibrational states are possible. In certain parametric regions, we demonstrate that the Nonlinear Schrödinger (NLS) equation predicts the corresponding modes fairly well. The electromechanical model we apply predicts accurately the conversion from the obtained mechanical energy to electrical energy observed in the experiments.

PACS numbers:

I. INTRODUCTION

Granular chains consist of closely packed arrays of particles that interact elastically [1]. The contact force can be tuned to yield near linear to purely nonlinear responses, and the effective stiffness properties can also be easily changed by modifying the material, geometry, or contact angle of the elements in contact [1]. This remarkable tunability has made the topic of granular chains an active research area over the past two decades (see the reviews [1–3]). Granular chains have been proposed for numerous applications such as shock and energy absorbing layers [4–7], actuating devices [8], acoustic lenses [9], acoustic diodes [10] and switches [11], as well as sound scramblers [12, 13]. Examples of fundamental studies include solitary waves [1, 2, 14, 15] and dispersive shocks [16, 17].

Time-periodic solutions have also been explored [3], and constitute one of the main focal points of this article. Time-periodic solutions which are also localized in space (so-called breathers) have been explored in a host of nonlinear lattice models during the 25 years since their theoretical inception, as has been summarized, e.g., in [18]. Examples include optical waveguide arrays or photorefractive crystals [19], micromechanical cantilever arrays [20], Josephson-junction ladders [21], layered antiferromagnetic crystals [22], halide-bridged transition metal complexes [23], dynamical models of the DNA double strand [24] and Bose-Einstein condensates in optical lattices [25]. In the context of granular chains, breathers have been studied in various settings, including monomers (chains where all particles are identical) [26], chains with defects [27], dimers (chains with a spatial periodicity of two) [28] and trimers and quadrimers (chains with a spatial periodicity of three and four respectively) [29]. Gap effects related to transient behavior of driven dissipative granular chains have also been studied [30]. Time-periodic solutions of damped-driven granular chains (including breathers, but not exclusively) have been explored in monomers [31], defect chains [10], dimers [32] and trimers [33].

Despite the large volume of studies of time-periodic solutions in granular chains, there has been very little attention paid to the high amplitude time-periodic solutions that exist in these models, especially from an experimental perspective. For example, a common theme in the studies of damped-driven granular chains is the transition between low-amplitude time-periodic states to quasi-periodicity or chaos [10, 32, 33]. The focus of this article will be on the different vibrational states in damped-driven granular chains. Herein, we measure voltage variations

---

related to different force transmission between particles by embedding a piezoelectric sensor connected to a purely resistive load in one of the beads of the chain. The resulting power is then calculated as $P = V^2/R$, where V is the measured voltage drop over the resistor which has resistance R. We are particularly interested in states that yield larger values of voltage (and hence power). We identify various vibrational states and characterize them through experiments, numerical simulations and, in certain parametric regions, theory for a large range of input (i.e. driving) frequencies. While fundamentally interesting in their own right, the spontaneous emergence of such states under harmonically driven excitations could potentially prove promising towards energy harvesting applications. While systems incorporating nonlinearity or multiple modes have been shown to harvest energy more efficiently than ones based on linear oscillators (see, e.g., the prototypical work of [34], but also the books [35–37] for a comprehensive treatment of energy harvesting), these two concepts have not yet been combined for the purpose of energy harvesting. We note that by making use of solitary waves, the granular chain has been proposed as an energy harvesting device [38–40]. In this article we demonstrate that combination of nonlinearity and multiple modes of the granular chain lead to the possibility of high energy states for a broad range of input frequencies. In the future, different systems, bearing resemblance to granular chains, could be engineered to exploit similar nonlinear phenomena as the one described in this paper for use in energy harvesting applications.

The manuscript is organized as follows: in Secs. II and III we describe the experimental and theoretical set-ups respectively. The main results are presented in Sec. IV where we demonstrate that the granular chain has the possibility for high energy states for a broad range of input frequencies. In Sec. V we provide an analytical prediction for the voltage production based on a long-wave length approximation. We provide concluding remarks and future directions in Sec. VI.

II. EXPERIMENTAL SETUP

Figure 1 shows the experimental setup. The chain consists of 21 identical chrome steel spheres (see Table I for their mechanical properties and dimensions). These spheres are aligned using four polytetrafluoroethylene (PTFE) rods to constrain the particles' transverse motions while allowing their longitudinal vibrations with minimum friction against the supporting rods. The PTFE rods are mounted on the upper and lower stainless steel blocks to reduce the vibration effect of the rods (see the upper inset of Fig. 1).

We apply 10 N force to the chain for static pre-compression using a spring and linear stage system [43]. The chain is dynamically excited by two piezo actuators (Piezomechanik PSt 150/5/7 VS10) in contact with the first and last beads. A common excitation signal is generated using a function generator (Agilent 33220A), and it is sent to each actuator after being amplified through separate amplifiers (Piezomechanik LE 150/100 EBW) as shown in Fig. 1. This enables us to excite both ends of the chain out-of-phase. We measure the dynamic responses of the chain using a laser Doppler vibrometer (LDV, Polytec OFV-534). The vibrometer is placed in an automated sliding rail at a slanted angle (45°), collecting the velocity profiles at specific particle spots. In this study, the localization and garnering of mechanical energy at the center of the chain is of particular interest. Therefore, besides the non-contact LDV method, we position a contact-based piezoelectric sensor bead at the center of the chain. For this, we fabricate a custom-made particle that embeds a lead zirconate titanate (PZT) disc between two halves of stainless steel spheres as shown in the lower inset of Fig. 1 [12]. The dimensions and properties of the PZT disc are in Table I. Note that the total mass and contact stiffness of the sensor bead are the same with that of the other beads, such that this bead can be treated as a regular particle in numerical simulations. The PZT disc is connected with an electronically controlled resistance box (IET OS-260), which is set to 3kΩ in this study. We measure the voltage applied to the resistor using an external oscilloscope.

We excite and test the granular chain in two different ways. One approach is that we excite the chain using a single frequency harmonic signal over a span of 0.1s. Given the speed of propagating waves in the chain, this is a period long enough to make the system reach a stationary state. We take the last 0.01s data to characterize the steady state response of the chain at specific frequencies. In this way, we use harmonic signals with the frequency from 6.00 kHz to 7.89 kHz at a 30 Hz interval. The other approach is that in a single round of testing, we dynamically sweep the frequencies from high (7.50 kHz) to low (6.50 kHz) ranges with 50 Hz step. Here, we run each frequency for 0.05s and take the last 0.01s data in each frequency interval. In both experiments, the amplitude of the excitation is consistent with $a = 0.11\mu m$. We perform each test three times to calculate their averages and standard deviations.
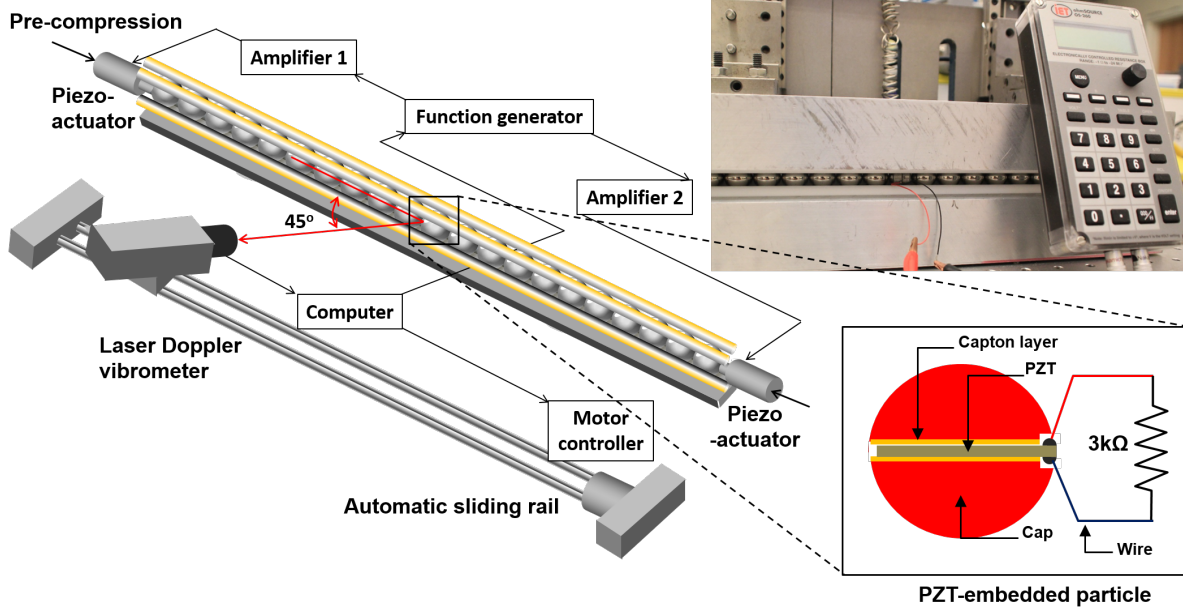
FIG. 1: Schematic of the experimental setup. The upper inset shows a digital image of the system, while the lower inset illustrates a schematic of the piezoelectric ceramic (PZT)-embedded sensor bead.

Mechanical Parameters			Electrical Parameters		
Bead Mass	M	28.2 g	Piezo Constant	d_{33}	360×10^{-12} m/V
Bead Young's Modulus	E	200 GPa	Piezo Permittivity	ϵ^T	141664×10^{-12} F/m
Bead Radius	r	9.53 mm	Piezo Compliance	S^E	72 GPa^{-1}
Bead Poisson's Ratio	ν	0.3	Piezo Disc Area	A	283.5 mm
Damping Coefficient	τ	5 ms	Piezo Thickness	d	0.3 mm
			Resistance	R	$3\ k\Omega$

TABLE I: Values of the electromechanical parameters. Mechanical properties are taken from nominal numbers available online and provided by vendors [42], and geometrical dimensions are measured.

III. THEORETICAL SETUP

In order to explore the theoretical model of interest for our system, we briefly touch upon the granular chain [1]. The force resulting from the deformation of two (identical) spherical particles in contact is described by the classical Hertz law $F(x) = \gamma[x]_+^{3/2}$, where x is the overlap between the two particles, $\gamma = \frac{E\sqrt{2r}}{3(1-\nu^2)}$ is the bead material parameter and the bracket is defined by $[\cdot]_+ = \max(0, \cdot)$. See [41] for the full original derivation of this contact law and [2] for a brief "back of the envelope" calculation. It is straight-forward then to obtain the equations of motion for a chain of particles in contact. The model for the spatially homogeneous and damped-driven variant has the form,

$$M\ddot{u}_n = \gamma[\delta_0 + u_{n-1} - u_n]_+^{3/2} - \gamma[\delta_0 + u_n - u_{n+1}]_+^{3/2} - \frac{M}{\tau}\dot{u}_n, \quad n \in [1, N] \tag{1}$$

where N is the number of beads in the chain, $u_n = u_n(t) \in \mathbb{R}$ is the displacement of the n-th bead from equilibrium position at time t, M is the bead mass and δ_0 is an equilibrium displacement induced by a static load $F_0 = \gamma\delta_0^{3/2}$ (this implies that when the chain is at rest, the overlap between adjacent particles is δ_0). The form of dissipation is a dash-pot (controlled by τ) which can be interpreted as the friction between individual grains and PTFE rods. This form of dissipation has been utilized in the context of granular chains in several previous works [10, 31, 33], but it is worth noting that works such as [16] (see also [44], as well as [45]) considered the internal

friction caused by contact interaction between grains. We consider out-of-phase harmonic boundary actuation,

$$u_0 = a\cos(2\pi f_b t), \qquad u_{N+1} = -a\cos(2\pi f_b t) \tag{2}$$

where a and f_b represent the amplitude and frequency of the actuation respectively. We insert a piezoelectric (PZT) sensor in the middle bead since a voltage will be produced upon its deformation. In particular, a PZT sensor with area A and thickness d is used. To model the electromechanical system, we make use of the constitutive relations describing piezoelectric materials, which in the IEEE standard notation have the form [46],

$$D = \epsilon^T E + d_{33} T, \tag{3a}$$
$$S = d_{33} E + s^E T, \tag{3b}$$

where D is the electric displacement, E is the electric field, T is the stress and S is the strain. ϵ^T is the permittivity, s^E is the inverse of the Young's modulus and d_{33} is the piezoelectric constant. For the parameters used in this study, see Table I. If we assume that the electrical and mechanical quantities are uniform throughout the PZT sensor (with area A and thickness d) then we infer $Q = DA$ where Q is the total electric charge on the electrodes, $E = V/d$ where V is the voltage between the electrodes and $f = AT$, where f is the total force. Using these relations, we may rewrite Eq. (3) as

$$\begin{pmatrix} Q \\ \Delta \end{pmatrix} = \begin{pmatrix} C & d_{33} \\ d_{33} & 1/K_a \end{pmatrix} \begin{pmatrix} V \\ f \end{pmatrix} \tag{4}$$

where $\Delta = Sd$ is the displacement (total extension) of the PZT, $K_a = \frac{A}{s^E d}$ is the piezo stiffness and $C = \frac{\epsilon^T A}{d}$ is the piezo capacitance. Inverting Eq. (4) yields,

$$\begin{pmatrix} V \\ f \end{pmatrix} = \frac{K_a}{C(1-k^2)} \begin{pmatrix} 1/K_a & -d_{33} \\ -d_{33} & C \end{pmatrix} \begin{pmatrix} Q \\ \Delta \end{pmatrix} \tag{5}$$

where $k^2 = \frac{d_{33}^2}{s^E \epsilon^T}$ is the electromechanical coupling factor.

The equations of motion consisting of positions q and velocities $\dot{q}$ of a mechanical system are the Euler-Lagrange equations of the Lagrangian $\mathcal{L}_m$ [47],

$$0 = \frac{d}{dt}\left(\frac{\partial \mathcal{L}_m}{\partial \dot{q}}\right) - \frac{\partial \mathcal{L}_m}{\partial q},$$

with $\mathcal{L}_m = T^*(\dot{q}) - \mathcal{V}(q)$ where T^* and $\mathcal{V}$ are, respectively, the kinetic and potential energy of the mechanical system. This formalism can also be applied to electrical systems [46]. Using the flux-linkage coordinate λ and voltage $\dot{\lambda} := V$ the equations of motion describing the electrical system are the Euler-Lagrange equations of the Lagrangian

$$\mathcal{L}_e = W_e^*(\dot{\lambda}) - W_m(\lambda)$$

where W_e^* is called the electrical co-energy (which is analogous to the kinetic energy of a mechanical system) and W_m is the magnetic potential (which is analogous to the potential energy of a mechanical system). For example, a capacitive element with capacitance C in a circuit will be represented by the electrical co-energy $W_e^*(\dot{\lambda}) = \frac{1}{2}C\dot{\lambda}^2$. The electrical energy associated with the capacitive element $W_e(Q)$ is related to the co-energy through the Legendre transformation $W_e(Q) = \dot{\lambda}Q - W_e^*(\dot{\lambda})$, where Q is the charge. Using the constitutive relation for a linear capacitor $C\dot{\lambda} = Q$ yields the energy stored in the capacitor $W_e(Q) = \frac{1}{2C}Q^2$. While this formulation is fairly trivial in the case of a stand-alone electrical system, it is quite natural when deriving the equations of motion for an electromechanical system. In this case, the Lagrangian will be the sum of the contributions from the mechanical system and the electrical system [46],

$$\mathcal{L} = T^* - \mathcal{V} + W_e^* - W_m.$$

In what follows, we assume the corresponding magnetic potential energy W_m is negligible, since e.g. we will not consider inductive elements. For a piezoelectric element the total power will be the sum of the electrical power $\dot{\lambda}\dot{Q}$ and mechanical power $f\dot{\Delta}$. Thus, to compute the electric energy W_e, we have

$$\frac{dW_e}{dt} = \dot{\lambda}\dot{Q} + f\dot{\Delta}.$$

Upon substitution of $V = \dot{\lambda}$ and f from Eq. (5) we see that the above is the total differential of

$$W_e = \frac{Q^2}{2C(1-k^2)} - \frac{d_{33}K_a}{C(1-k^2)}Q\Delta + \frac{K_a\Delta^2}{2(1-k^2)}.$$

We can obtain the co-energy by making use of the Legendre transformation,

$$W_e^*(\Delta, \dot{\lambda}) = \dot{\lambda}Q - W_e(\Delta, Q)$$

which, after additional calculation, finally leads to,

$$W_e^*(\Delta, \dot{\lambda}) = W_e^*(\Delta, V) = C(1-k^2)\frac{V^2}{2} + d_{33}K_aV\Delta - K_a\frac{\Delta^2}{2}. \tag{6}$$

We treat the bead with the embedded PZT as two half beads attached by a "spring" (i.e. the PZT) [48], where each half has mass $M/2$. We assume that these halves are located at sites m and $m+1$. Thus, the total extension of the PZT is $\Delta = \delta_1 + u_{m+1} - u_m$, where δ_1 is the initial extension of the PZT due to any static force. With these assumptions, the Lagrangian of the electromechanical system has the form,

$$\mathcal{L} = \sum_n \frac{1}{2}M_n\dot{u}_n^2 + \sum_{n\neq m}\left[-\gamma\frac{5}{2}[\delta_0 + u_n - u_{n+1}]_+^{5/2}\right] + W_e^*(\Delta, V)$$

where W_e^* is defined by (6) and $M_n = M/2$ for $n = m, m+1$ and $M_n = M$ otherwise. The equations of motion can be obtained starting from this Lagrangian:

$$M\ddot{u}_n = \gamma[\delta_0 + u_{n-1} - u_n]_+^{3/2} - \gamma[\delta_0 + u_n - u_{n+1}]_+^{3/2} - \frac{M}{\tau}\dot{u}_n, \quad n \notin \{m, m+1\} \tag{7a}$$

$$\frac{M}{2}\ddot{u}_m = \gamma[\delta_0 + u_{m-1} - u_m]_+^{3/2} - K_a(\delta_1 + u_m - u_{m+1}) - d_{33}K_aV - \frac{M}{2\tau}\dot{u}_m, \tag{7b}$$

$$\frac{M}{2}\ddot{u}_{m+1} = K_a(\delta_1 + u_m - u_{m+1}) - \gamma[\delta_0 + u_{m+1} - u_{m+2}]_+^{3/2} + d_{33}K_aV - \frac{M}{2\tau}\dot{u}_{m+1}, \tag{7c}$$

$$C(1-k^2)\dot{V} = -d_{33}K_a(\dot{u}_m - \dot{u}_{m+1}) - \frac{V}{R} \tag{7d}$$

where $F_0 = K_a\delta_1$. The non-conservative terms appearing above are phenomenological terms added to account for the presence of damping. We model mechanical dissipation as a dash-pot (i.e. the terms $\frac{M}{\tau}\dot{u}_m$, $\frac{M}{2\tau}\dot{u}_m$, $\frac{M}{2\tau}\dot{u}_{m+1}$ in Eqs. (7a)-(7c) respectively). To convert voltage to power, we connect the electrodes with a purely resistive load R, which results in the non-conservative term V/R in Eq. (7d). Finally, we assume that the chain is finite in length, where the boundaries are given by Eq. (2).

It is also worth mentioning that many studies on granular chains use embedded PZT elements to deduce the force applied on particles in a granular chain [1]. Indeed, it is only recently that the use of laser vibrometry has been introduced to probe the dynamics of the granular chain [49]. Typically, the voltage response measured from the PZT is calibrated empirically in order to obtain a force. Equation (7) provides a more precise description of how the voltage relates to the applied force on a given particle. Moreover, it describes how the electrical system can affect the dynamics of the mechanical system, and that for large voltage responses, the dynamics can be severely altered. Although this aspect is outside the scope of the present article, it would be an interesting direction for future studies.

A. Linear Regime

For dynamic displacements satisfying $\frac{|u_n - u_{n+1}|}{\delta_0} \ll 1$ we can expand the Hertzian forcing term in a Taylor series,

$$\gamma[\delta_0 + y]^{3/2} \approx \gamma\delta_0^{3/2} + K_2y + K_3y^2 + K_4y^3, \qquad K_2 = \frac{3}{2}\gamma\delta_0^{1/2}, \quad K_3 = \gamma\frac{3}{8}\delta_0^{-1/2}, \quad K_4 = -\gamma\frac{3}{48}\delta_0^{-3/2}. \tag{8}$$

Thus, the linear equations (where $K_3 = K_4 = 0$) have the form,

$$M_n\ddot{u}_n = \beta_n(u_{n-1} - u_n) - \beta_{n+1}(u_n - u_{n+1}) - \rho_nV - \frac{M_n}{\tau}\dot{u}_n, \tag{9a}$$

$$RC(1-k^2)\dot{V} = -d_{33}K_aR(\dot{u}_m - \dot{u}_{m+1}) - V \tag{9b}$$

where,

$$\beta_n = \begin{cases} K_2 & n \neq m \\ K_a & n = m \end{cases} \qquad M_n = \begin{cases} M & n \neq m, m+1 \\ M/2 & \text{otherwise} \end{cases} \qquad \rho_n = \begin{cases} d_{33} K_a & n = m \\ -d_{33} K_a & n = m+1 \\ 0 & \text{otherwise} \end{cases} . \tag{10}$$

The linear resonances of this system will be determined by Eq. (9a), which we view as a homogeneous mass-spring system with two adjacent defects located at sites m and $m+1$. Ignoring the mechanical and electrical damping terms, one can show that there is a continuous (discrete) band of modes for an infinite (finite) system $f \in [0, f_0]$ where $f_0 = \sqrt{K_2/M}/\pi$ is the cut-off frequency of the homogeneous chain. The presence of the defects introduces two additional modes, which correspond to the defects being in- or out-of-phase. They can be approximated respectively as [50],

$$f_{defect}^{(1)} \approx \frac{1}{2\pi} \sqrt{\frac{1}{M^2}(s_1 \pm \sqrt{s_2})}, \tag{11}$$

$$f_{defect}^{(2)} \approx \frac{1}{2\pi} \sqrt{\frac{1}{M^2}(s_3 \pm \sqrt{s_4})} \tag{12}$$

where $s_1 = 2K_2 M$, $s_2 = 2K_2^2 M^2$, $s_3 = s_1 + 2K_a M$ and $s_4 = -4[2K_2 K_a + K_2(2K_a + K_2)]M^2/2 + 4[K_a M + K_2 M]^2$. In-phase motion of the two defects will result in no voltage production (see Eq. (7d)), and thus $f_{defect}^{(1)}$ will not be relevant for our purposes. On the other hand, since $K_2 \ll K_a$, out-of-phase motion of the defects will occur for frequencies much larger than the maximum frequency obtainable in experiments (in the case of the parameters of Table I the largest frequency is $f_{defect}^{(2)} \approx 349.63$ kHz, whereas $f_0 = 7.765$ kHz). Thus, since these defect modes (either due to their nature or due to their frequency range) cannot produce significant voltage in the considered granular configuration, we resort to exciting several lower frequency (global) modes in order to produce a voltage response.

Considering once again the electrical and mechanical damping, and an external harmonic excitation, we seek to compute the linear steady-state response. We use the ansatz $u_n = \phi_n e^{i2\pi f_b t}$ and $V = \phi_v e^{i2\pi f_b t}$ and define $u_0 = -u_{N+1} = a e^{i2\pi f_b}$, where N is the number of nodes (corresponding to $N-2$ beads and two bead halves) and where a is the excitation amplitude and f_b is the excitation frequency. We solve the resulting system of complex algebraic equations for $\{\phi_n, \phi_v\}$, where the steady-state solution is then the real part of $\phi_n e^{i2\pi f_b t}$ and $\phi_v e^{i2\pi f_b t}$. Thus, if the natural response of the host structure is known, the material properties of the particles can in principle be selected such that the resonant peaks match the natural response. In a chain of cylindrical particles in contact, it has been demonstrated recently that the stiffness K_2 can be easily tuned dynamically by alternating the contact angle of cylinders [51].

IV. MAIN RESULTS

Since we are driving the chain harmonically, natural solutions to look for are time-periodic ones. We compute a solution with period $T_b = 1/f_b$ with high precision by finding roots of the map $\mathbf{x}(T_b) - \mathbf{x}(0)$, where $\mathbf{x}(T_b)$ is the solution of Eq. (7) at time T_b with initial condition $\mathbf{x}(0)$. Roots of this map (and hence time-periodic solutions of Eq. (7)) are found via Newton iterations. An initial guess for the Newton iterations can be provided by the steady-state solution of the linearized equations (9). Once a solution is found a parametric continuation is performed. In this study, we keep all parameters fixed, and vary either the excitation amplitude a or the excitation frequency f_b. For example, the solid lines in Fig. 2(a) are found by performing a pseudo-arclength continuation in the frequency f_b of the time-periodic solutions. Spectral stability of these solutions is determined through the computation of Floquet multipliers corresponding to the Hill's equation that results from linearizing the equations of motion about a time-periodic solution [18]. A solution where all Floquet multipliers have modulus less than unity is asymptotically stable (solid blue lines in Fig. 2(a)), marginally stable if the module of all multipliers is equal to unity, and unstable otherwise. We classify the instabilities as either real if the associated Floquet multiplier is purely real (dashed red lines in Fig. 2(a)), or oscillatory if it has real and imaginary parts (dash-dot green lines in Fig. 2(a)). We make this distinction since oscillatory instabilities are typically smaller in magnitude (see for example [31, 33]) and oscillatory instabilities suggest the presence of Neimark-Sacker bifurcations and hence of quasi-periodic solutions. Finally, the emergence of a purely real Floquet multiplier with modulus greater than unity signals the bifurcation of additional period 1 solutions and solutions of higher periodicity [18]. For purposes of
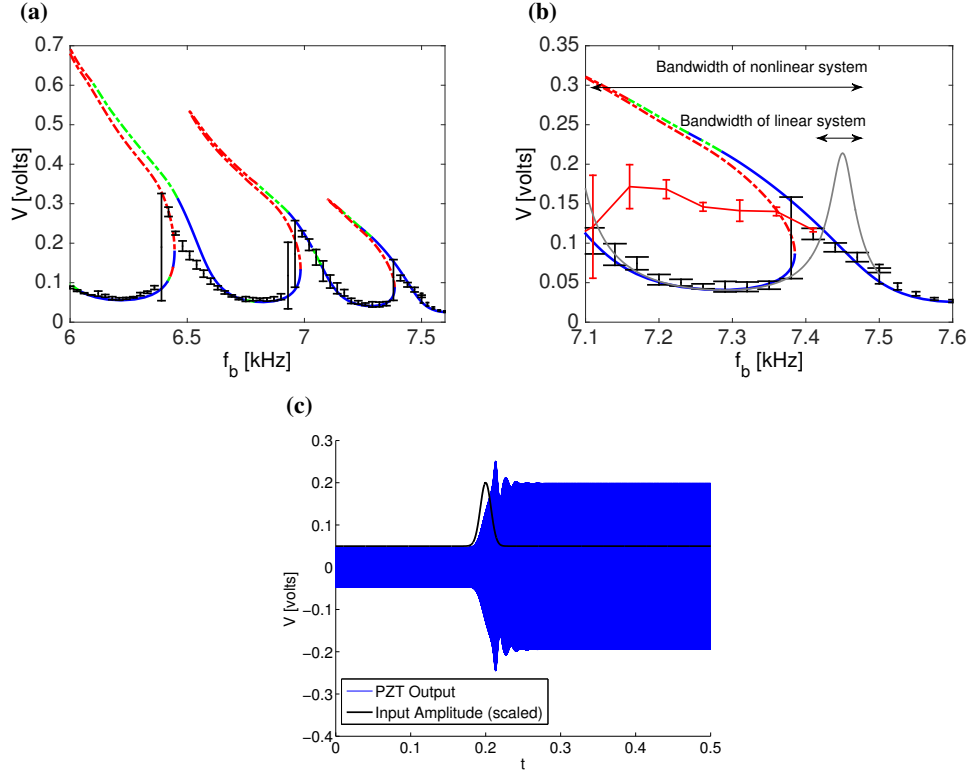
FIG. 2: (Color online) **(a)** Voltage amplitude of time-periodic solutions of Eq. (7) vs driving frequency and a fixed driving amplitude of $a = 0.11\mu m$ (blue, red and green lines). The color is associated with the stability properties of the respective solutions (see details in the text). The experimental voltages shown (black markers with error bars) represent the average amplitude of the voltage over the final 10 ms of a 100 ms run. Each experimental run was initially at rest. Three experiments per marker were performed to obtain statistics. **(b)** Zoom of panel (a) in the 7.1-7.6 kHz region. The thick red error bars correspond to an experiment where the actuation frequency was decreased dynamically (every 0.05 s). The values shown represent the average voltage amplitude over the final .01 s before the frequency was updated. The linear response is also shown (light gray line). **(c)** Voltage response for an amplitude of $a = 0.11\mu m$ and $f_b = 7.32$ kHz with a short amplitude burst where the maximum amplitude is increased by a factor of 1.5 (solid black line).

clarity and in connection to the principal scope of the present manuscript, quasi-periodic solutions and solutions of higher order periodicity are not shown in Fig. 2(a-b). It should be noted, however, that the bifurcation of such solutions is indeed connected to the stability changes observed in Fig. 2(a-b).

As a first step, we validate the proposed model by comparing the above described time-periodic solutions of Eq. (7) to experimental results. Starting from the zero state (i.e. when the chain is at rest), the chain is driven at the boundaries with the excitation amplitude and frequency being fixed. We let the experiment run for 100 ms and then compute the average amplitude of the voltage over the final 10 ms. If there is a stable periodic solution nearby, the 100 ms is typically long enough to allow the solution to reach that solution. We use the theoretically predicted values of all parameters with the exception of the precompression (through $F_0 = 13.7$ N), which is used to match the linear resonant frequencies of the experiment and theory. The compliance of the PZT $S^E = 36\,\mathrm{GPa}^{-1}$ and the electromechanical coupling parameter $k = 0.87$ are modified to obtain better agreement of the voltage output. The experimental measurements match the theoretical predictions quite well in regions of asymptotic stability, see Fig. 2(a), which validates the model in Eq. (7). In Fig. 2 the voltage is shown since this is the quantity directly measured from the experiments, however, the power can be computed using the formula $P = V^2/R$ where in this study $R = 3\,\mathrm{k}\Omega$.

The effect of the nonlinearity in the system is apparent in Fig. 2(a), where the resonant peaks have bent (in this case toward lower frequencies), such that there are high amplitude states for a large range of frequencies. The bending trend of the resonant peaks as the driving amplitude varies is shown in Fig. 3, see also [52]. This, in conjunction with the multi-modal nature of our system, implies the possibility of high amplitude states for a broad range of frequencies. However, if the system starts from the zero state, and the excitation conditions are fixed, the low amplitude state (which is typically stable) will be approached. See for example the experimental measurements

in Fig. 2(a). However, if the excitation frequency is changing dynamically (in this case from high to low), it is possible to access the high amplitude states. In Fig. 2(b) experimental measurements are shown starting from the zero state as black markers with error bars and experimental measurements that have a frequency that changes dynamically from high to low frequency are shown as thick red markers with error bars. In the latter, one sees that higher amplitudes have been achieved, although the agreement between theory and experiment is not as good as in the low amplitude regime. While the precise reasons for the disagreement observed in the larger amplitude regime are not fully understood, we propose two possible explanations: (i) in experiments it is difficult to reach a steady state dynamic response. This is because the excitation of the system is changed dynamically throughout experiments and the system's quality factor is very high. Moreover, the Floquet multipliers lie within but near to the unit circle, thereby requiring relatively long times for the system to settle to a steady-state behavior. (ii) For larger amplitude excitations, other effects ignored by our model might be playing a larger role in the dynamics, potentially enhancing the disparity between our numerical and experimental observations. Particle rotation is one example. The fact that the contact points of the particles cannot be perfectly aligned in experiments due to the clearance between the beads and the support rods is another. This is likely to result in dynamic buckling of the chain under high amplitude motion. It is also likely that additional (nonlinear) forms of dissipation affect the particle motion (such as damping due to sphere-to-sphere contact [16, 44], elastic (but also plastic) deformation, and damping due to rotation). While taking into consideration these numerous effects in the model may yield a better quantitive prediction, our simple model provides the qualitatively correct prediction: higher amplitude states are possible if the frequency is dynamically varying. We note that Fig. 2(a) shows comparison of experiment and theory of low amplitude states in the stationary regime, which shows very good agreement.

Another possibility to transition into a high amplitude state is to apply a short amplitude burst to the excitation, see Fig. 2(c). This aspect could be particularly useful for applications where being in a higher amplitude state is desirable, and is worthy of future investigation in its own right.
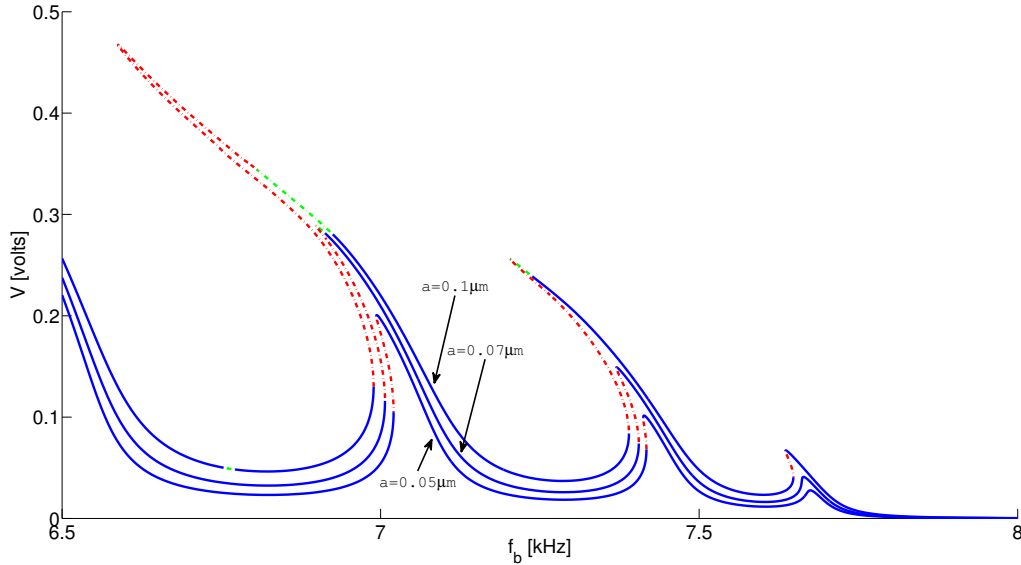

FIG. 3: (Color online) Bifurcation diagrams corresponding to the voltage as a function of the actuation frequency f_b and for various values of the actuation amplitude of $a = 0.05\,\mu$m, $a = 0.07\,\mu$m and $a = 0.1\,\mu$m are presented with smooth curves and increasing order (see the arrows). Note that the blue segments correspond to stable parametric regions while the red and green ones correspond to real and oscillatory unstable parametric regions, respectively (see text).

A useful benchmark for this system is its linearized counterpart. Imagine that one can construct a linear system that has a resonant frequency near the dominant frequency of some vibrating host structure, and that the parameters are tuned such that the voltage production at full width at half maximum (FWHM) is sufficient for the application of interest. In Fig. 2(b) the linear prediction is shown as the light gray line. If the host structure vibrates at a resonant frequency (i.e. 7.45kHz), then both the linear system and our nonlinear system would meet the voltage production requirements. If the excitation frequency differs by about .05 kHz from the linear resonant frequency (due to e.g. mistuning), and the system is always starting from zero, then our nonlinear system and the linear system will both fail to meet the minimum requirement. If in addition the excitation
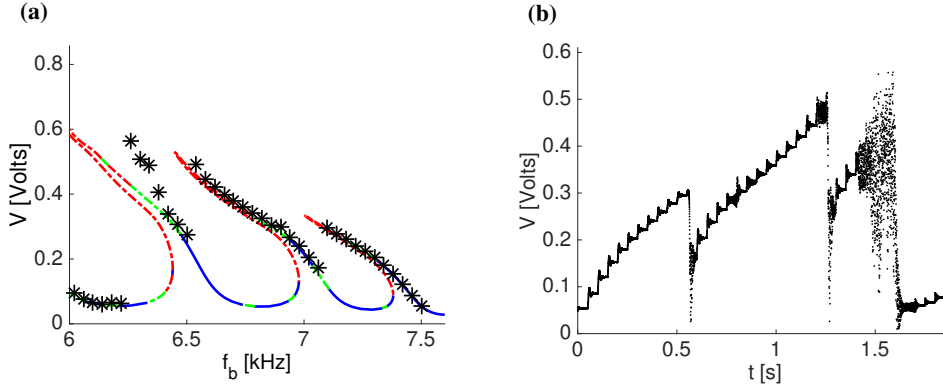
FIG. 4: (Color online) **(a)** Voltage amplitude of time-periodic solutions of Eq. (7) vs driving frequency and a fixed driving amplitude of $a = 0.12\mu m$ (blue, red and green lines). The color is associated with the stability properties of the respective solutions (see details in the text). The black markers correspond to a simulation where the actuation frequency was decreased dynamically (every .05 s) starting at $f_b = 7.5$ kHz. The values shown represent the average voltage amplitude over the final .01 s before the frequency was updated. **(b)** Time series of the voltage response. For clarity, only local maxima of the time series are shown.

frequency is changing dynamically, then the nonlinear system has the potential to meet the minimum voltage requirement, whereas the linear system would fail. For example, the FWHM of the linear response is approximately 0.1 volts with a corresponding bandwidth of 0.05 kHz. The effective bandwidth of the nonlinear response in the window shown in Fig. 2(b) with voltages exceeding the FWHM (0.1 volts) is 0.3 kHz. This represents a 500% increase in bandwidth. For the chosen system size ($N = 22$), there are 10 resonant peaks located at $\{1.1026, 2.1887, 3.2257, 4.1997, 5.0826, 5.8674, 6.5330, 7.0656, 7.4510, 7.6831\}$ kHz, each of which bends toward lower frequencies. The qualitative features shown in Fig. 2(b) can be found around each of these frequencies implying the possible broadband capabilities of this system. Note, in a traditional single oscillator, there can only be one resonant peak. Since our system has multiple-modes, and hence multiple resonant peaks, we can exploit the multiple modes to obtain an even broader response (broader than e.g. Fig. 2(b)). For example, Fig. 4 shows the result of dynamically decreasing the excitation frequency from 7.5 kHz to 6.1 kHz with the actuation amplitude fixed to be $a = 0.12\mu$m. Since the linear resonant peaks located at 6.5330 kHz, 7.0656 kHz and 7.4510 kHz are each bent toward lower frequencies, the effective response is even broader than when considering frequencies near a single mode (as was the case in Fig. 2(b)) or if considering a single oscillator (see e.g. the insets of Fig. 2(a-c) of [52] for the case of a single granular particle). This is because in the absence of the bent resonant peaks, the response will be of low amplitude. It is worth noting that, even though the high amplitude states may be unstable in certain regions of the frequency, the corresponding instabilities are rather weak. Thus, over transient dynamical regimes, it is possible to be near these large amplitude states for relatively long times, as is the case in Figs. 2 and 4. While the introduction of additional modes can increase the bandwidth of the system, it will also enhance the effect of damping. This could be compensated by e.g. introducing multiple sensors throughout the chain to increase the power output.

V. NLS APPROXIMATION

The Hamiltonian limit of Eq. (1) corresponds to $\tau \to \infty$ and $a \to 0$. While clearly this limit is an over-simplification of the problem, this limit can be useful towards understanding the full electromechanical system of Eq. (7) in certain parametric regions, as we detail below. The connection between the Hamiltonian system and the damped-driven variant can be most easily seen by performing a continuation in driving amplitude a and fixing all other parameters. In Fig. 5(a) an amplitude continuation is shown for various values of τ. For small values of a and sufficiently large values of τ one can see a low amplitude state, (the near linear state which is "dictated" by the actuators) and two high amplitude nonlinear states that meet and collide in a saddle-node bifurcation at some critical value of the driving amplitude a_{cr}; see the arrows of Fig. 5(a) and also [32]. Since $a_{cr} \ll 1$, the solution at the saddle-node is "as close as possible" to the corresponding Hamiltonian solution. In that same limit (of $\tau \to \infty$ and $a \to 0$) the nonlinear Schrödinger (NLS) equation can be derived from Eq. (1) written in terms of the negative
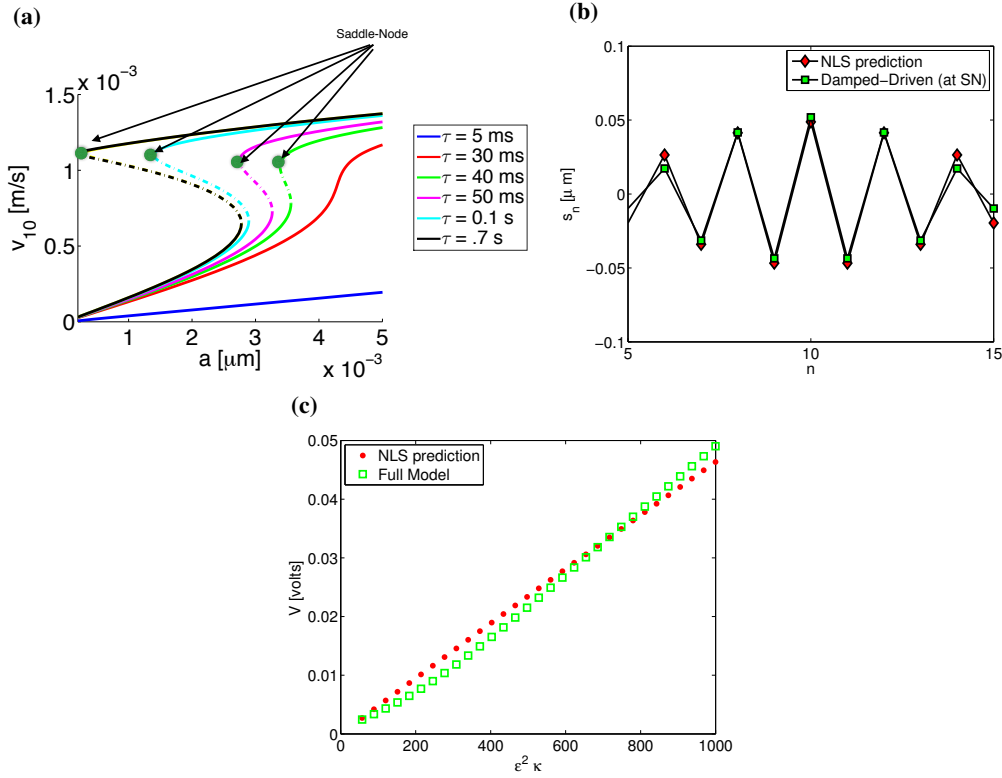
(a)

(b)

(c)

FIG. 5: (Color online) **(a)** Continuation in driving amplitude a of time-periodic solutions of Eq. (1) for a fixed driving frequency of $f_b = 7.29$ kHz and various dissipation values. The maximum velocity of 10th particle is shown. The saddle-node (SN) bifurcations which progressively approach the NLS limit as $a \to 0$ (for τ sufficiently large) are labeled by the arrows. **(b)** Comparison of the NLS approximation (red diamonds) and corresponding time-periodic solution of Eq. (7) (green square) with a low dissipation associated with $\tau = 0.7$s **(c)** Steady-state amplitude of the voltage as predicted by Eq. (22) (red circles) and the actual values given through Eq. (7) (green squares) using the experimentally determined value of the parameter $\tau = 0.5$ ms.

strain variable $y_n = u_{n-1} - u_n$, [26, 53]. In particular, one defines the multiple-scale ansatz,

$$y_n(t) \approx \psi_n(t) := \varepsilon A(X,T)e^{i(k_0 n + \omega_0 t)} + \text{c.c.} + \text{h.o.t}\,, \quad X = \varepsilon(n + ct), \quad T = \varepsilon^2 t, \qquad (13)$$

where $\varepsilon \ll 1$ is a small parameter, effectively parameterizing the solution amplitude (and also its inverse width). The substitution of this ansatz into the equations of motion and equation of the various orders of ϵ leads to the dispersion relation $\omega_0 = \omega(k_0) := 2\sqrt{K_2/M} \sin(k_0/2)$, the group velocity relation $c = \omega'(k_0)$, and the nonlinear Schrödinger equation,

$$i\partial_T A(X,T) + \nu_2 \partial_X^2 A(X,T) + \nu_3 A(X,T)|A(X,T)|^2 = 0, \qquad (14)$$

where $\nu_2 = -\omega''(k_0)/2 > 0$ and

$$\nu_3 = \frac{K_3^2}{K_2^2}\tilde{\gamma} + \frac{3K_4}{2K_2}\omega(k_0) < 0, \qquad (15)$$

while

$$\tilde{\gamma} = \frac{\omega(k_0)}{2}\left(\frac{\omega(2k_0)}{2\omega(k_0) - \omega(2k_0)} - \frac{\omega(2k_0)}{2\omega(k_0) + \omega(2k_0)} \right.$$
$$\left. + \frac{2\omega'(0)}{\omega'(k_0) - \omega'(0)} - \frac{2\omega'(0)}{\omega'(k_0) + \omega'(0)}\right). \qquad (16)$$

The NLS equation is an integrable equation and has several exact solutions, such as the bright or (the relevant for our setting) dark soliton [54]. For the coefficients corresponding to the Taylor expansion of the Hertz contact force,

see Eq. (8), the NLS equation features a self-defocusing nonlinearity. As such, the dark soliton is an exact solution of Eq. (14). Using the dark soliton as the envelope function, we have the following approximation,

$$y_n(t) = 2\varepsilon(-1)^{n+1}\sqrt{\frac{\kappa}{\nu_3}}\tanh\left(\sqrt{\frac{-\kappa}{2\nu_2}}\epsilon(n-x_0)\right)\cos(\omega_b t) \qquad k_0 = \pi,\ \omega_0 = 2\sqrt{K_2/M},\ c = 0 \qquad (17)$$

where $\omega_b = \omega_0 + \kappa\epsilon^2$ is the frequency of oscillation, $\kappa < 0$ is a fixed but arbitrary parameter and $X_0 = \epsilon x_0$ is an arbitrary spatial translation; see [26] for more details.

We seek to maximize how much the bead with the PZT element is squeezed:

$$s_m(t) := u_{m-1} - u_{m+1} = y_m + y_{m+1}$$

where m is the location of the PZT element. This quantity in the NLS approximation becomes:

$$s_n(t) = 2\epsilon(-1)^n\sqrt{\frac{\kappa}{\nu_3}}\left(\tanh\left(\sqrt{\frac{-\kappa}{2\nu_2}}\epsilon(n+1-x_0)\right) - \tanh\left(\sqrt{\frac{-\kappa}{2\nu_2}}\epsilon(n-x_0)\right)\right)\cos(\omega_b t) \qquad (18)$$

$$\approx 2\epsilon^2(-1)^n\sqrt{\frac{\kappa}{\nu_3}}\left(1 - \tanh^2\left(\sqrt{\frac{-\kappa}{2\nu_2}}\epsilon(n-x_0)\right)\right)\cos(\omega_b t). \qquad (19)$$

Thus, the profile of the squeeze is localized at the center of the chain, see Fig. 5(b). If we take m to be at the center of the chain, and choose the actuation amplitude to correspond to the saddle-node bifurcation (see e.g. Fig. 5(a)) we will have an analytical approximation, increasingly valid in the limit of $\tau \to \infty$ and $a \to 0$ of how much the PZT bead is squeezed. To compute the corresponding voltage, we can solve the following equation,

$$\frac{M}{2}\ddot{u}_m = \gamma[\delta_0 + y_m]_+^{3/2} - K_a(\delta_1 + u_m - u_{m+1}) - d_{33}K_aV - \frac{M}{2\tau}\dot{u}_m, \qquad (20a)$$

$$\frac{M}{2}\ddot{u}_{m+1} = K_a(\delta_1 + u_m - u_{m+1}) - \gamma[\delta_0 + y_{m+1}]_+^{3/2} + d_{33}K_aV - \frac{M}{2\tau}\dot{u}_{m+1}, \qquad (20b)$$

$$RC(1-k^2)\dot{V} = -d_{33}K_aR(\dot{u}_m - \dot{u}_{m+1}) - V \qquad (20c)$$

where y_m, y_{m+1} is given by Eq. (17). For out-of-phase actuation in a chain of odd length, we expect the solution to be symmetric about the center bead, and hence we pick $x_0 = 1/2$ in Eq. (17) and $m = 0$ (for an infinite chain we assume $m = 0$ is the center), which leads to,

$$y_m(t) = y_{m+1}(t) = \alpha\cos(\omega_b t) := y(t), \qquad \alpha := 2\epsilon\sqrt{\frac{\kappa}{\nu_3}}\tanh\left(\sqrt{\frac{-\kappa}{2\nu_2}}\epsilon/2\right).$$

Since $y = \mathcal{O}(\epsilon) \ll \delta_0$, we expand the forcing terms in a Taylor series (see Eq. (8)), and then we define $z = u_m - u_{m+1}$, which leads to

$$\frac{M}{2}\ddot{z} + 2K_az + \frac{M}{2\tau}\dot{z} + 2d_{33}K_aV = 2(K_2\,y(t) + K_3\,y(t)^2 + K_4\,y(t)^3), \qquad (21a)$$

$$RC(1-k^2)\dot{V} = -d_{33}K_aR\dot{z} - V \qquad (21b)$$

which is a damped-driven linear ODE which can be solved exactly. While the full solution is cumbersome to express, the leading order term to the steady-state amplitude of the voltage is easily found. Thus, we finally arrive at the following approximation of the amplitude of the voltage,

$$V_{amp} = \frac{\alpha 4K_2\omega_b}{M\sqrt{(4K_a/M - \omega_b^2)^2 + (\omega_b/\tau)^2}}\frac{d_{33}K_aR}{\sqrt{1 + (CR\omega_b(1-k^2))^2}} \qquad (22a)$$

$$f_b = \frac{\omega_0 + \kappa\epsilon^2}{2\pi} \qquad (22b)$$

$$a = \varepsilon\sqrt{\frac{\kappa}{\nu_3}}. \qquad (22c)$$

To compute the driving amplitude a we made use of Eq. (17) and the approximation $|y_n| = 2|u_n|$ for $|n| \to \infty$. Although the approximation (22) is only valid in the limit of zero damping, it performs fairly well using the experimentally measured value of $\tau = 5\,\text{ms}$ for small values of $\omega_b - \omega_0 = \epsilon^2\kappa$ (i.e. for those close to the band edge), see Fig. 5(c). We note that this approximation can only be employed for the special combinations of actuation frequency and drive given by Eqs. (22b)-(22c) respectively. Hence, it is evident that in the limit where the NLS approximation becomes relevant, the voltage between the electrodes of the PZT can not only be numerically computed but also analytically approximated.

VI. CONCLUSIONS AND FUTURE DIRECTIONS

We considered a harmonically driven 1D granular chain with an embedded piezoelectric sensor (a PZT) at the center of the chain. Vibrational states of the nonlinear system, which were identified by measuring the voltage output of the PZT sensor, were found to exist for much broader range of input frequencies when compared to the linearized counterpart of this system. The electromechanical model we derived provided good agreement to the experimentally observed values under both static and dynamic driving frequency, although it may be less accurate for large amplitude (more highly nonlinear) states. The electromechanical model provides an insightful description of how the electrical system can affect the dynamics of the mechanical system, and could be useful for future studies in granular chains that utilize PZT sensors to deduce force, without relying on calibration factors. The NLS equation also provided an analytical prediction of the voltage production for certain combinations of driving frequency and amplitude that compared favorably to numerical simulations. While this study focused on out-of-phase boundary excitations, we suspect that other harmonic excitation conditions (where e.g. the phase difference between the two driving frequencies is arbitrary) will yield qualitatively similar results, although the optimal location for the PZT may no longer be the center. Thus, an interesting future direction would be to study a chain in which different particles contain a PZT and the chain is subject to various driving boundary excitations (not necessarily out-of-phase). Optimizing the relevant mechanism and identifying the relation between optimal voltage output at different sites as a function of phase would certainly be of interest to future work.

We believe this study lays a foundation for future investigations of energy harvesting in spatially extended nonlinear dynamical systems, identifying their capability for more broadband harvesting, but also raising some of their limitations including the scale of the phenomenon and the partial lack of (numerical) control of the output of the mechanism for larger amplitudes/high nonlinearities. While the granular chain itself may not be ideal for energy harvesting purposes, it demonstrates that the combination of multiple modes and nonlinearity can lead to the possibility of different vibrational states (including high energy ones) for a broad range of input frequencies.

Acknowledgments

[1] V. F. Nesterenko, *Dynamics of Heterogeneous Materials* (Springer-Verlag, New York, NY, 2001).

[2] S. Sen, J. Hong, J. Bang, E. Avalos, and R. Doney, Phys. Rep. **462**, 21 (2008).

[3] G. Theocharis, N. Boechler, and C. Daraio, in *Phononic Crystals and Metamaterials*, Ch. 6, Springer Verlag, (New York, 2013).

[4] C. Daraio, V. F. Nesterenko, E. B. Herbold, and S. Jin, Phys. Rev. Lett. **96**, 058002 (2006).

[5] J. Hong, Phys. Rev. Lett. **94**, 108001 (2005).

[6] F. Fraternali, M. A. Porter, and C. Daraio, Mech. Adv. Mat. Struct. **17**(1), 1 (2010).

[7] R. Doney and S. Sen, Phys. Rev. Lett. **97**, 155502 (2006).

[8] D. Khatri, C. Daraio, and P. Rizzo, SPIE **6934**, 69340U (2008).

[9] A. Spadoni and C. Daraio, Proc Natl Acad Sci USA, **107**, 7230, (2010).

[10] N. Boechler, G. Theocharis, C. Daraio, Nature Materials **10**, 665 (2011).

[11] F. Li, P. Anzel, J. Yang, P.G. Kevrekidis, and C. Daraio, Nature Communications **5**, 5311 (2014).

[12] C. Daraio, V. F. Nesterenko, E. B. Herbold, and S. Jin, Phys. Rev. E **72**, 016603 (2005).

[13] V. F. Nesterenko, C. Daraio, E. B. Herbold, and S. Jin, Phys. Rev. Lett. **95**, 158702 (2005).

[14] C. Coste, E. Falcon, and S. Fauve, Phys. Rev. E **56**, 6104 (1997).

[15] K. Ahnert and A. Pikovsky, Phys. Rev. E **79**, 026209 (2009).

[16] E. B. Herbold and V. F. Nesterenko, Phys. Rev. E **75**, 021304 (2007); see also: A. Rosas, A.H. Romero, V.F. Nesterenko, and K. Lindenberg Phys. Rev. Lett. **98**, 164301 (2007).

[17] A. Molinari and C. Daraio, Phys. Rev. E **80**, 056602 (2009).

[18] S. Flach and A. V. Gorbach, Phys. Rep. **467**, 1 (2008).

[19] F. Lederer, G.I. Stegeman, D.N. Christodoulides, G. Assanto, M. Segev, and Y. Silberberg, Phys. Rep. **463**, 1 (2008).

[20] M. Sato, B.E. Hubbard, and A.J. Sievers, Rev. Mod. Phys. **78**, 137 (2006).

[21] P. Binder, D. Abraimov, A.V. Ustinov, S. Flach, and Y. Zolotaryuk, Phys. Rev. Lett. **84**, 745 (2000);
E. Trías, J.J. Mazo, and T.P. Orlando, Phys. Rev. Lett. **84**, 741 (2000).

[22] L.Q. English, M. Sato, and A.J. Sievers, Phys. Rev. B **67**, 024403 (2003);
U.T. Schwarz, L.Q. English, and A.J. Sievers, Phys. Rev. Lett. **83**, 223 (1999).

[23] B.I. Swanson, J.A. Brozik, S.P. Love, G.F. Strouse, A.P. Shreve, A.R. Bishop, W.-Z. Wang, and M.I. Salkola, Phys. Rev. Lett. **82**, 3288 (1999).

[24] M. Peyrard, Nonlinearity **17**, R1 (2004).

[25] O. Morsch and M. Oberthaler, Rev. Mod. Phys. **78**, 179 (2006).

[26] C. Chong, P.G. Kevrekidis, G. Theocharis, and C. Daraio, Phys. Rev. E. **87**, 042202 (2013).

[27] G. Theocharis, M. Kavousanakis, P. G. Kevrekidis, C. Daraio, M. A. Porter, and I. G. Kevrekidis, Phys. Rev. E **80**, 066601 (2009); S. Job, F. Santibanez, F. Tapia and F. Melo, Phys. Rev. E **80**, 025602 (2009).

[28] N. Boechler, G. Theocharis, S. Job, P. G. Kevrekidis, M. A. Porter and C. Daraio, Phys. Rev. Lett. **104**, 244302 (2010).

[29] C. Hoogeboom and P. G. Kevrekidis, Phys. Rev. E **86**, 061305 (2012).

[30] E.B. Herbold, J. Kim, V.F. Nesterenko, S.Y. Wang and C. Daraio, Acta Mech. **205**, 85 (2009).

[31] C. Chong, F. Li, J. Yang, M.O. Williams, I.G. Kevrekidis, P.G. Kevrekidis and C. Daraio, Phys. Rev. E **89**, 032924 (2014).

[32] C. Hoogeboom, Y. Man, N. Boechler, G. Theocharis, P. G. Kevrekidis, I. G. Kevrekidis and C. Daraio, Euro. Phys. Lett. **101** , 44003 (2013).

[33] E. G. Charalampidis, F. Li, C. Chong, J. Yang, P. G. Kevrekidis, Mathematical Problems in Engineering, **2015**, 830978 (2015).

[34] B. Marinkovic and H. Koser, Appl. Phys. Lett. **94**, 103505 (2009).

[35] A. Erturk, D. J. Inman, *Piezoelectric Energy Harvesting* (John Wiley & Sons Ltd., Chichester, UK, 2011).

[36] N. Elvin and A. Erturk (Eds.) *Advances in Energy Harvesting Methods* (Springer-Verlag, New York, NY, 2013).

[37] Stephen Beeby and Neil White (Eds.) *Energy Harvesting for Autonomous Systems* (Artech House, London, 2010).

[38] K. Li, P. Rizzo, J. of App. Phys. **117**, 215101 (2015).

[39] K. Li, P. Rizzo, J. Vib. Acoust. **137**, 041002 (2015).

[40] K. Li, P. Rizzo, J. of Sound Vib. **365**, 15–21 (2016).

[41] H. Hertz, J. Reine Angew. Math. **92**, 156–171 (1881).

[42] Stainless steel material property: `http://www.efunda.com/`, Piezoelectric ceramic property: `http://www.steminc.com/`

[43] F. Li, L. Yu and J. Yang, J. Phys. D: Appl. Phys. **46** 155106 (2013).

[44] L. Vergara Phys. Rev. Lett. **104**, 118001 (2010).

[45] R. Carretero-González, D. Khatri, Mason A. Porter, P. G. Kevrekidis, and C. Daraio Phys. Rev. Lett. **102**, 024102 (2009).

[46] A. Preumont, *Mechatronics: Dynamics of Electromechanical and Piezoelectric Systems* (Springer-Verlag, New York, NY, 2010).

[47] V.I. Arnol'd, *Mathematical Methods of Classical Mechanics* (Springer-Verlag, New York, NY, 1989).

[48] Joseph Lydon, *Nonlinear Effects in Granular Crystals with Broken Periodicity* PhD Thesis, California Institute of Technology, 2014.

[49] F. Li, L. Zhao, Z. Tian, L. Yu and J. Yang, Smart Mater. Struct. **22**, 035016 (2013).

[50] Y. Man, N. Boechler, G. Theocharis, P. G. Kevrekidis, and C. Daraio, Phys. Rev. E **85**, 037601 (2012).

[51] F. Li, C. Chong, J. Yang, P.G. Kevrekidis and C. Daraio, Phys. Rev. E **90**, 053201 (2014).

[52] J. Lydon, G. Theocharis, C. Daraio, Phys. Rev. E, **91**, 023208 (2015).

[53] G. Huang and B. Hu, Phys. Rev. B **57**, 5746 (1998).

[54] V.E. Zakharov and A.B. Shabat, J. Exp. and Theor. Phys. **34**, 62–69 (1972).